Dinuclear 2,4-di(pyridin-2-yl)-pyrimidine based ruthenium photosensitizers for hydrogen photo-evolution under red light.

Mira T. Gamache[1,2,3], Thomas Auvray[1], Garry S. Hanan[1], Dirk G. Kurth[2]

[1] *Département de Chimie, Université de Montréal, 1375 Avenue Thérèse-Lavoie-Roux, Montréal, Québec, H2V-03B, Canada*

[2] *Chemische Technologie der Materialsynthese, Julius-Maximilians-Universität Würzburg, Röntgenring 11, 97070 Würzburg, Germany*

[3] *Previously published under Mira T. Rupp*

Supporting information

S.I.-1 Instrumentation details

NMR experiments were performed on a Bruker AV-400 (^{1}H: 400 MHz and ^{13}C{^{1}H}: 101 MHz, Montréal, Canada) spectrometer, a Fourier 300 (^{1}H: 300 MHz and ^{13}C{^{1}H}: 75 MHz, Bruker Biospin, Rheinstetten, Germany) spectrometer or a Bruker Avance 500 (^{1}H: 500 MHz and ^{13}C{^{1}H}: 126 MHz, Montréal, Canada) spectrometer at 295 K. The chemical shifts are reported in ppm relative to the residual peak of the solvent as the internal standard. High-resolution mass spectrometry (HR-MS) was recorded either on a SYNAPT G2-Si spectrometer from Waters or on a Bruker Daltonics microQTOF spectrometer. Samples were ionized by electrospray ionization (ESI). UV-vis absorption spectra were recorded on an Agilent Cary6000i or Cary5000 UV-Vis-NIR spectrometer. Room-temperature emission and excitation spectra were recorded on a Jasco FP-8300 spectrometer equipped with a temperature control unit set to 20 °C or a LS 55 fluorescence spectrometer from PerkinElmer. Complexes were excited at 450 nm. The quantum yield was calculated using the dilute method[1] with $[Ru(Tolyltpy)_2](PF_6)_2$ as reference.[2] Solutions with an absorbance ranging between 0.04 and 0.09 were used and the following equation was applied to obtain the quantum yield value. The reported value is an average from different measurements.

$$\Phi_1 = \frac{S_1}{S_{ref}} \times \frac{A_{ref}}{A_1} \times \phi_{ref} \qquad \text{Equation S.I. 1}$$

S_1 and S_{ref} are the area of the emission peak, A_1 and A_{ref} the absorbance of the corresponding solution and Φ_1 and Φ_{ref} the quantum yield of our complex and of the reference, $[Ru(Tolyltpy)_2](PF_6)_2$, respectively.

For the luminescence lifetimes, an FLS920 fluorescence spectrometer (Edinburgh Instruments) using a 405 nm (room temperature measurements) or 508 nm (various temperature measurements) centered Hamamatsu diode laser was used. Sample solutions were degassed with nitrogen prior to measuring emission spectra or excited-state lifetimes. Electrochemical measurements were carried out in a three-electrode set-up with a glassy carbon disk (d=6mm) working electrode, a platinum coil as counter electrode and a platinum wire as pseudo-reference, using ferrocene as internal standard. The ferrocenium/ferrocene couple in acetonitrile was set to 0.40 V *vs*. SCE.[3] Measurements were made using a SP-50 BioLogic potentiostat interfaced to a computer equipped with the EC-lab software V11.21. Tetrabutylammonium hexafluorophosphate ($TBAPF_6$) was used as electrolyte in a concentration of 0.1 M. The concentration of the analyte was 1 mM for complexes **Ref1** and **Ref2**, 0.25 mM for complex **C1** and 0.5 mM for **C2**. The samples were purged by nitrogen before each measurement. The cyclic voltammograms were recorded with a sweep rate of 100 mV/s in dried acetonitrile (Acros, HPLC grade).

S.I.-2 NMR spectra

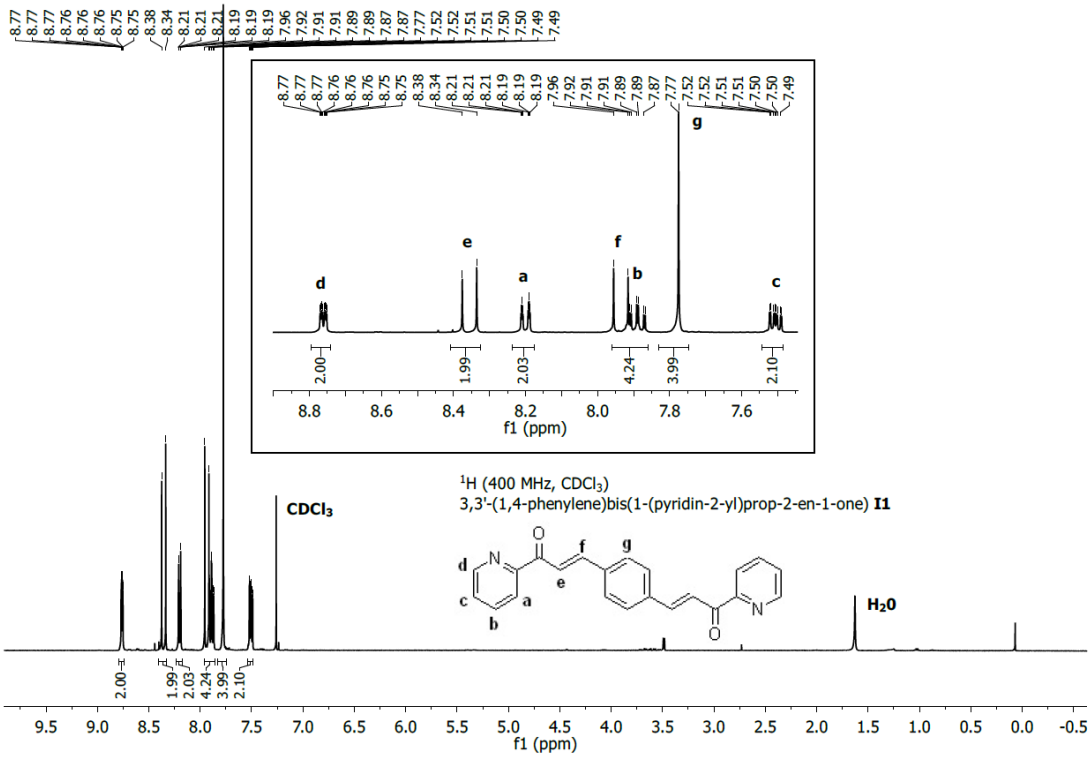

Figure S.I. 1. ^{1}H-NMR spectrum (400 MHz, $CDCl_3$) of 3,3'-(1,4-phenylene)-bis(1-(pyridine-2-yl)prop-2-en-1-one) **I1**.

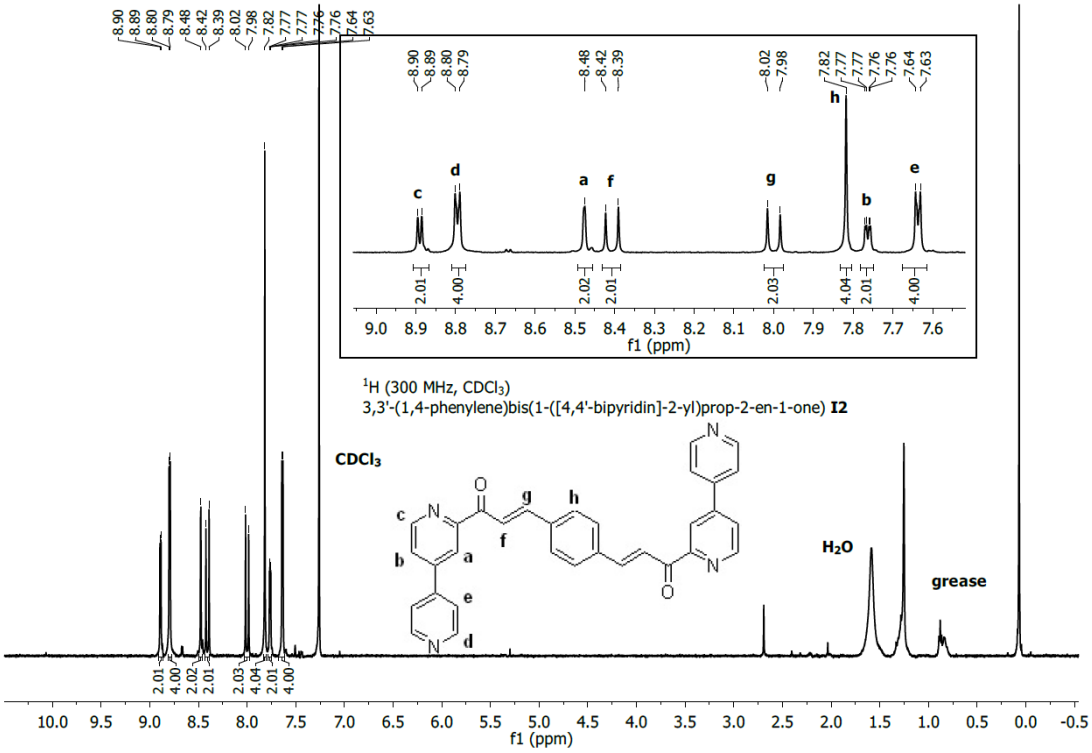

Figure S.I. 2. ^{1}H-NMR spectrum (300 MHz, $CDCl_3$) of 3,3'-(1,4-phenylene)-bis(1-([4,4'-bipyridin]-2-yl)prop-2-en-1-one) **I2**.

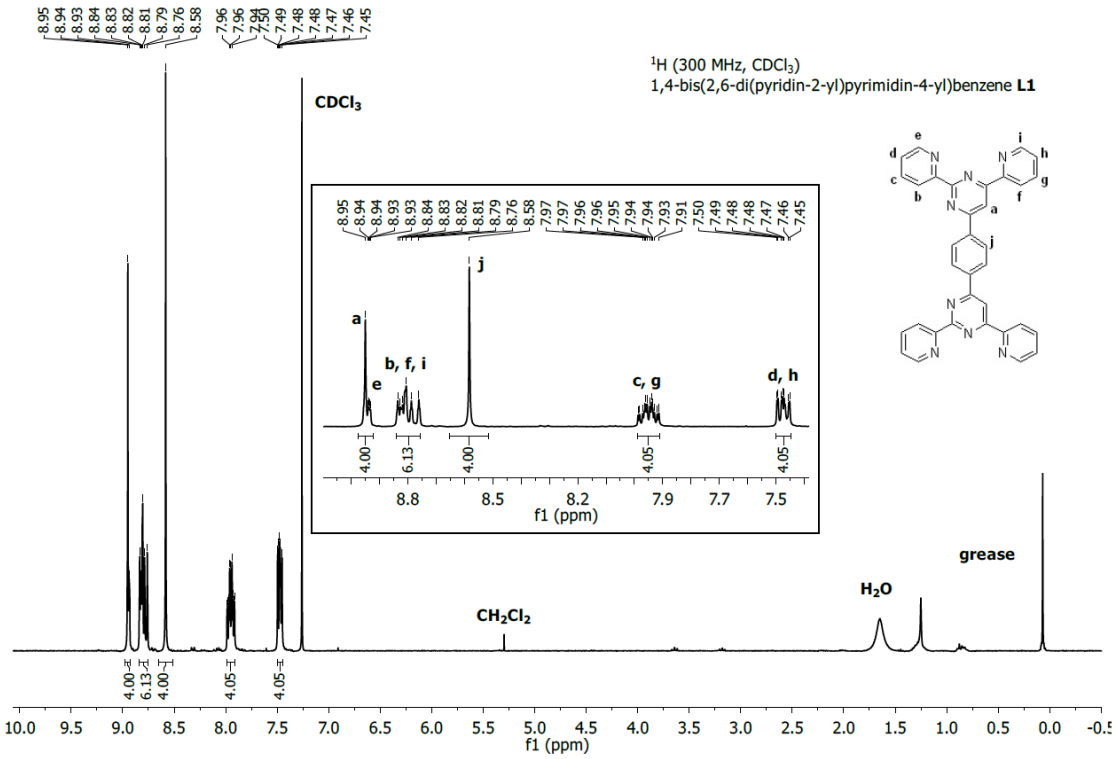

Figure S.I. 3. ^{1}H-NMR spectrum (300 MHz, $CDCl_3$) of 1,4-bis(2,6-di(pyridin-2-yl)pyrimidin-4-yl)benzene **L1**.

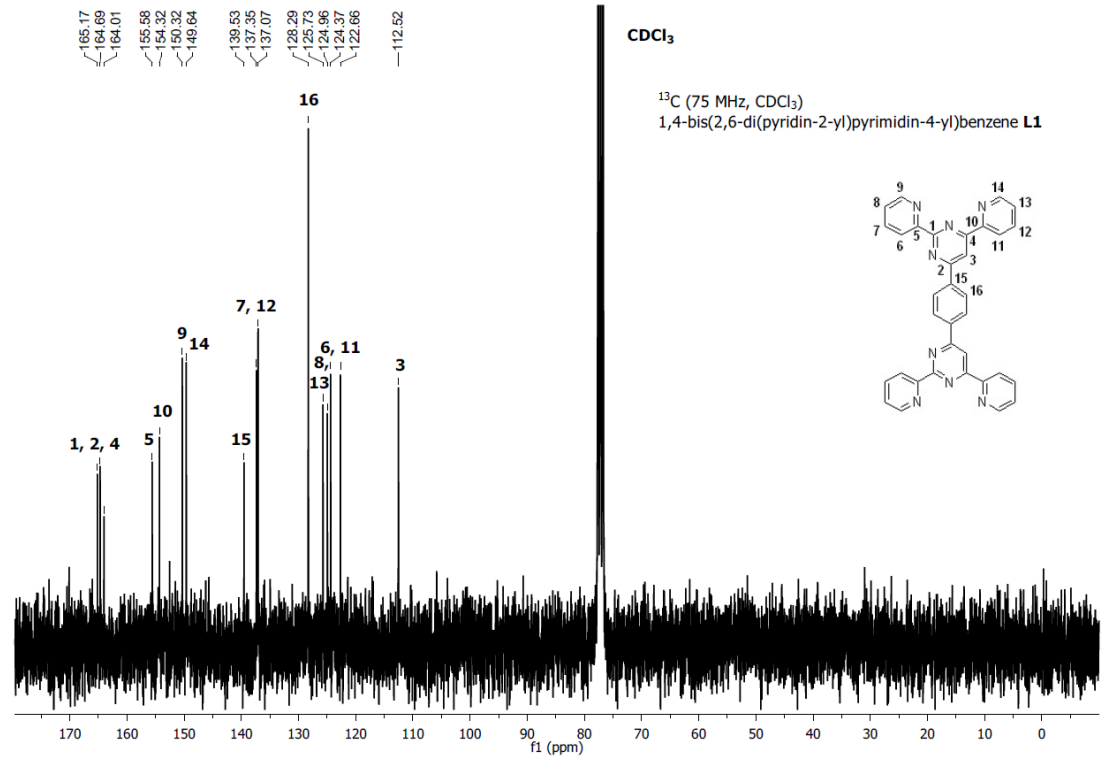

Figure S.I. 4. ^{13}C-NMR spectrum (75 MHz, $CDCl_3$) of 1,4-bis(2,6-di(pyridin-2-yl)pyrimidin-4-yl)benzene **L1**.

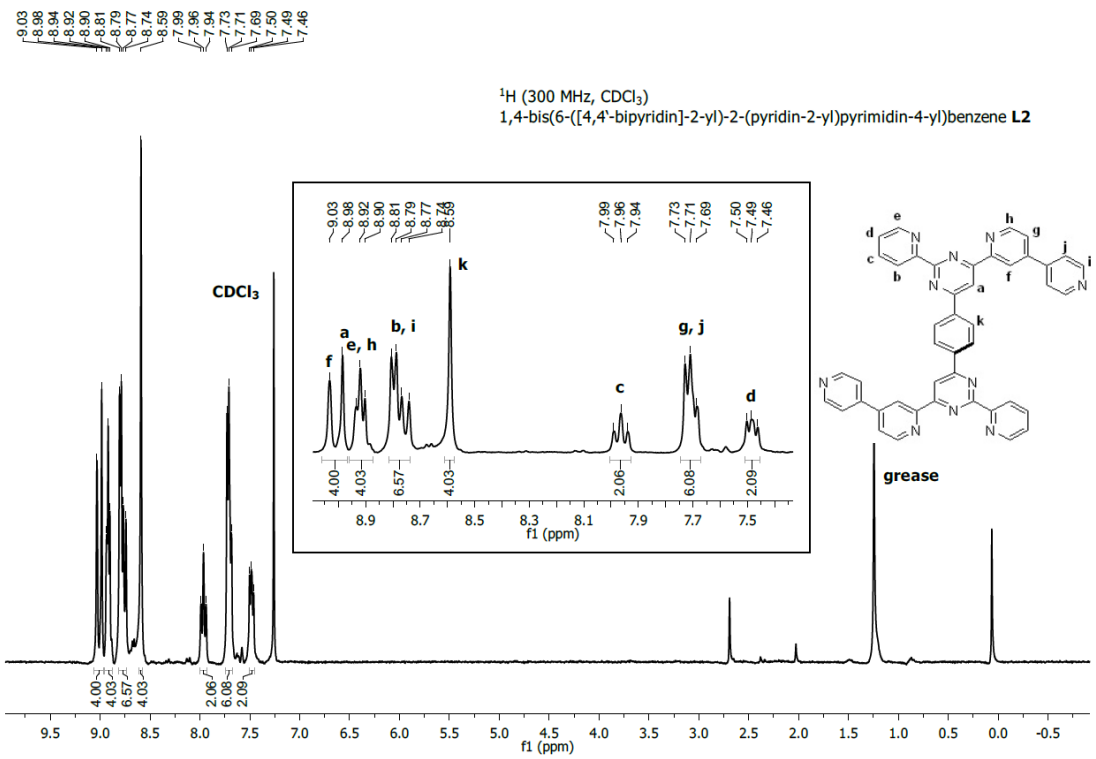

Figure S.I. 5. ^{1}H-NMR spectrum (300 MHz, $CDCl_3$) of 1,4-bis(6-([4,4'-bipyridin]-2-yl)-2-(pyridin-2-yl)pyrimidin-4-yl)benzene **L2**.

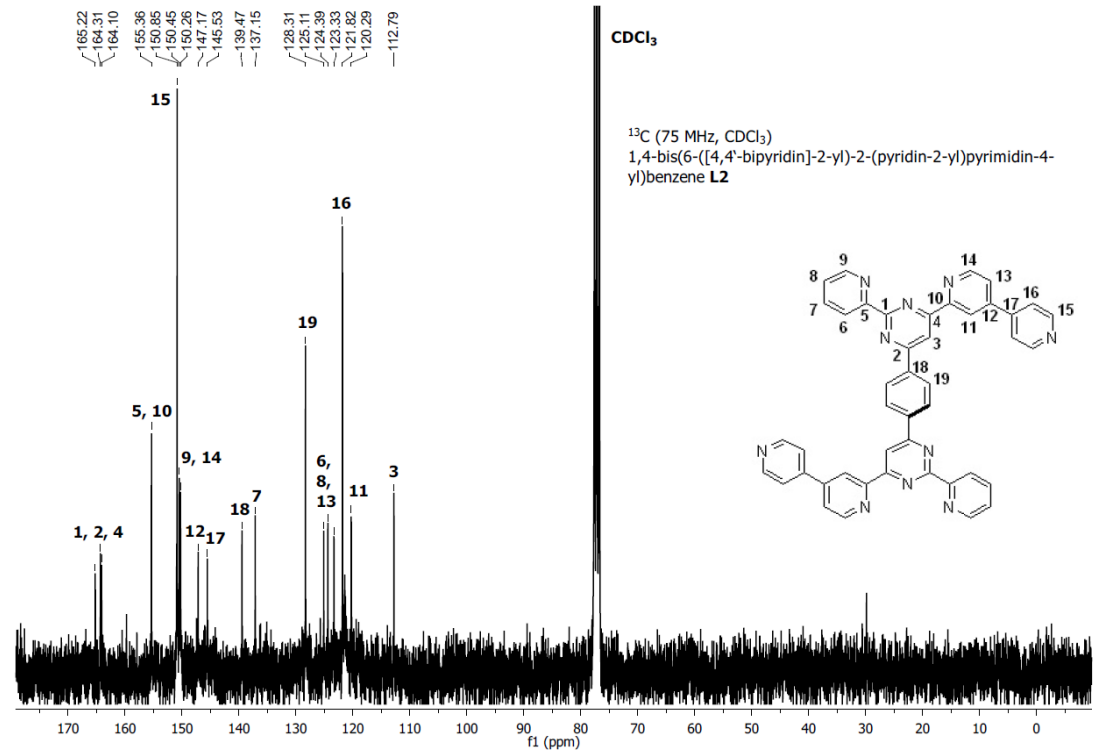

Figure S.I. 6. ^{13}C-NMR spectrum (75 MHz, $CDCl_3$) of 1,4-bis(6-([4,4'-bipyridin]-2-yl)-2-(pyridin-2-yl)pyrimidin-4-yl)benzene **L2**.

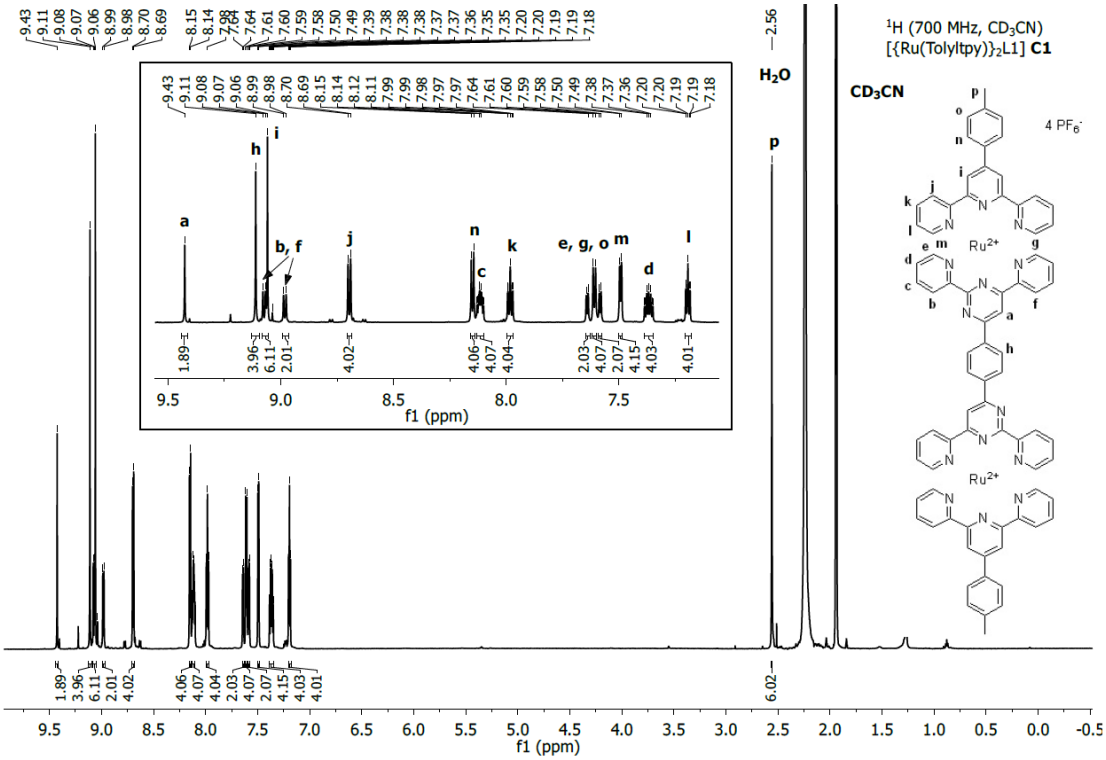

Figure S.I. 7. ^{1}H-NMR spectrum (700 MHz, CD_3CN) of [{Ru(Tolyltpy)}$_2$L1] **C1**.

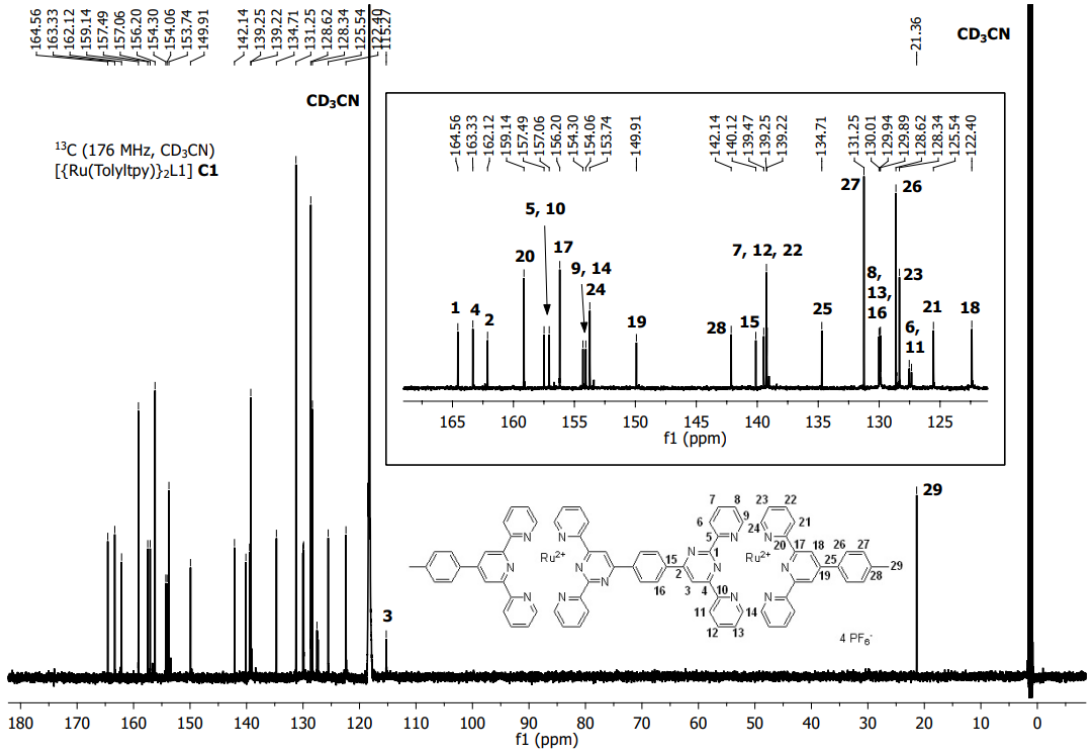

Figure S.I. 8. ^{13}C-NMR spectrum (176 MHz, CD_3CN) of [{Ru(Tolyltpy)}$_2$L1] **C1**.

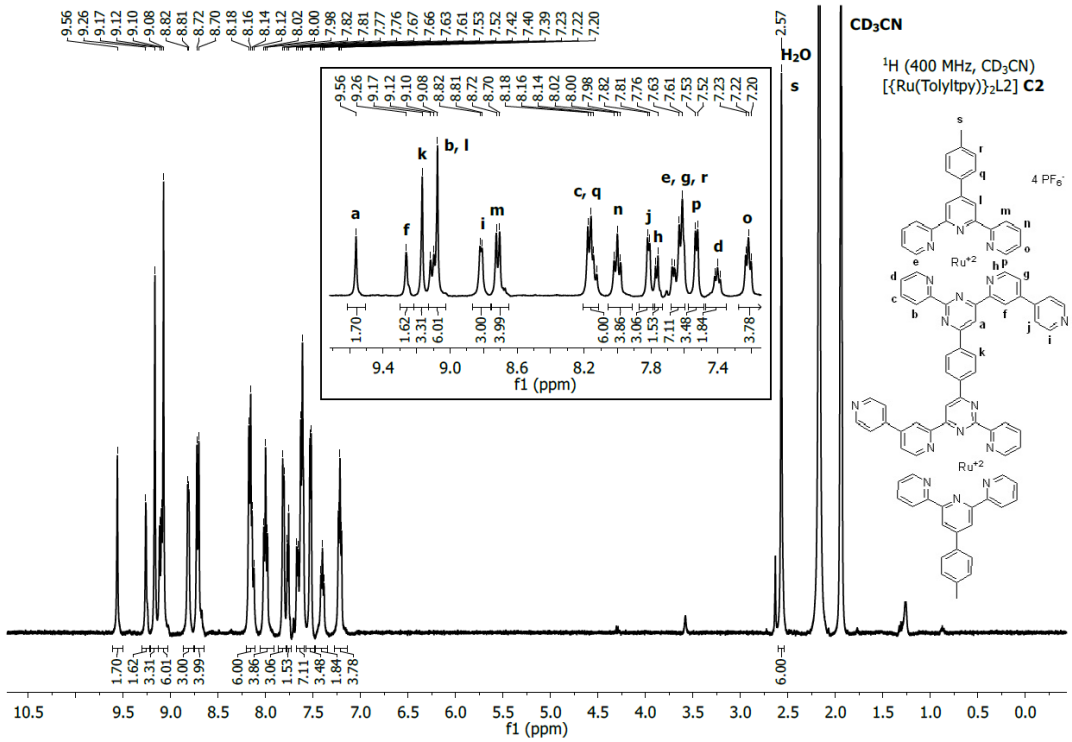

Figure S.I. 9. ^{1}H-NMR spectrum (400 MHz, CD_3CN) of [{Ru(Tolyltpy)}$_2$L2] **C2**.

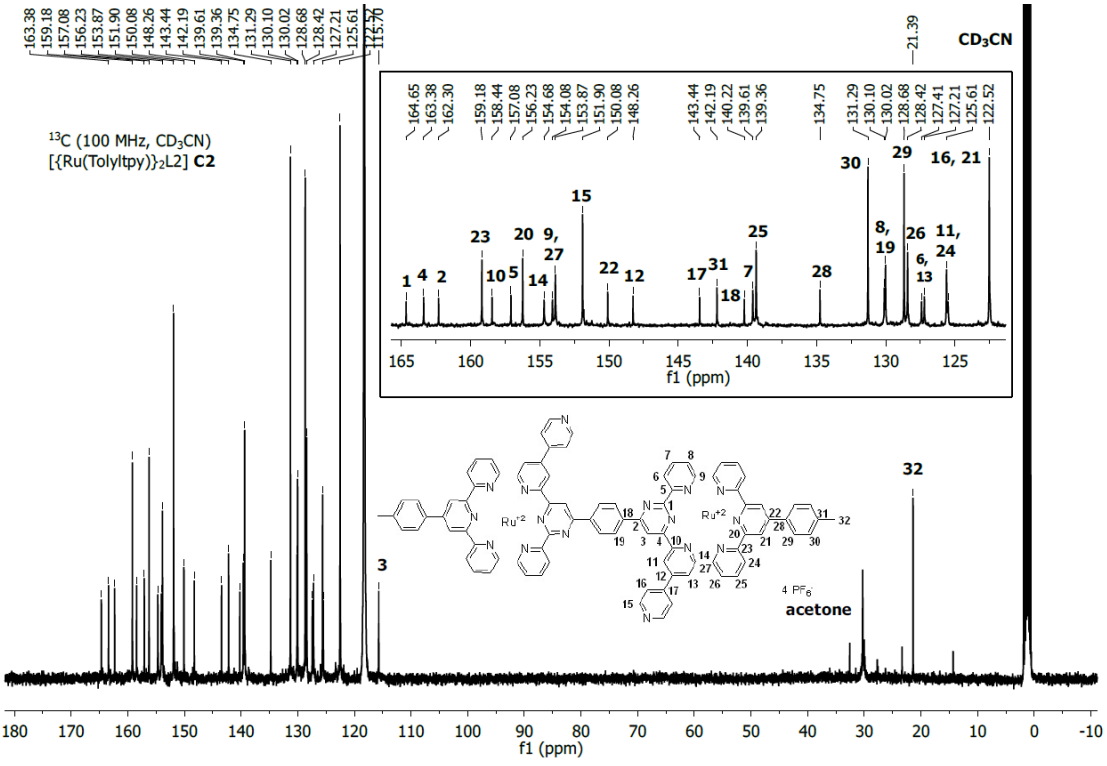

Figure S.I. 10. ^{13}C-NMR spectrum (100 MHz, CD_3CN) of [{Ru(Tolyltpy)}$_2$L2] **C2**.

S.I.-3 Photophysical properties

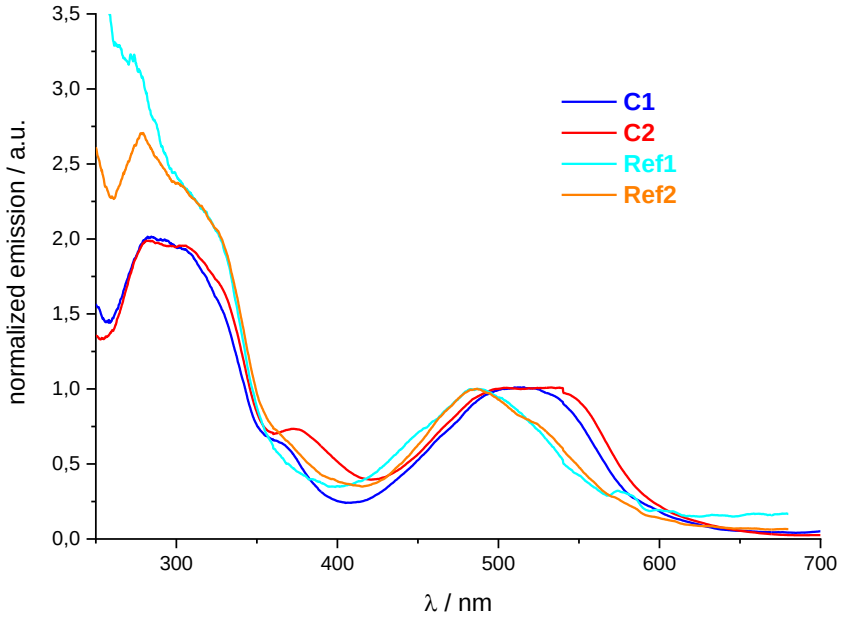

Figure S.I. 11. Excitation spectra of complexes **C1**, **C2**, **Ref1** and **Ref2** in inert-gas purged acetonitrile; spectra are normalized so that the emission intensity at the MLCT band is 1.

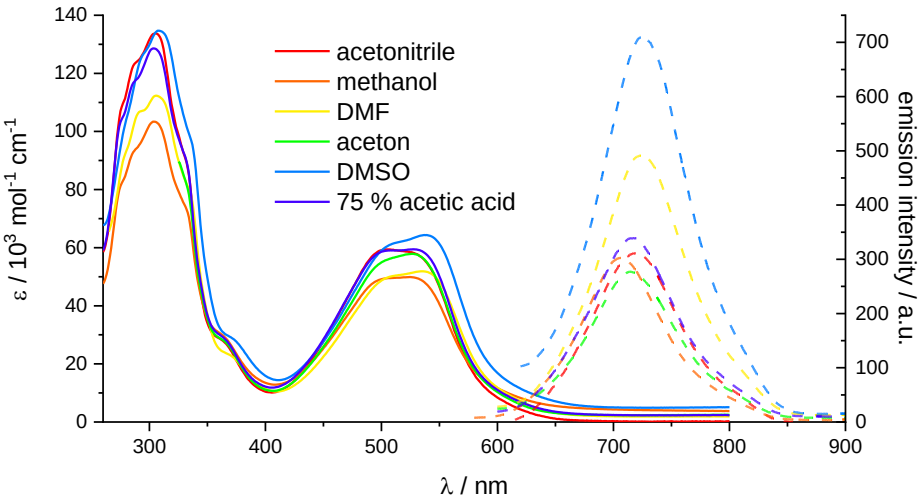

Figure S.I. 12. UV-vis absorption spectra (solid lines) and emission spectra (dashed lines) of complex **C1** in different inert-gas purged solvents; emission spectra are normalized with regard to the absorptivity of the sample solution at the excitation wavelength and the refractive index of the solvent.

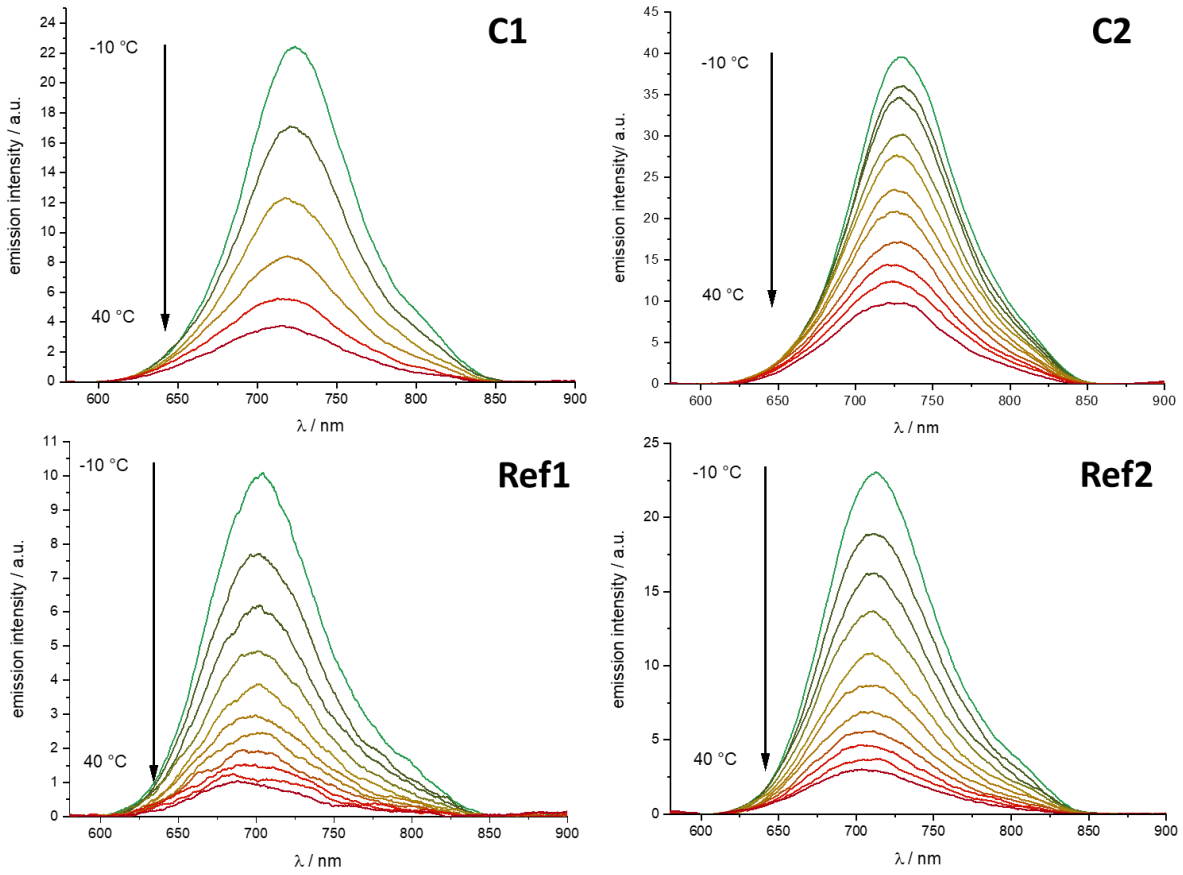

Figure S.I. 13. Emission spectra of complexes **C1**, **C2**, **Ref1** and **Ref2** in inert-gas purged acetonitrile at different temperatures; temperatures vary between +40 °C and -10 °C.

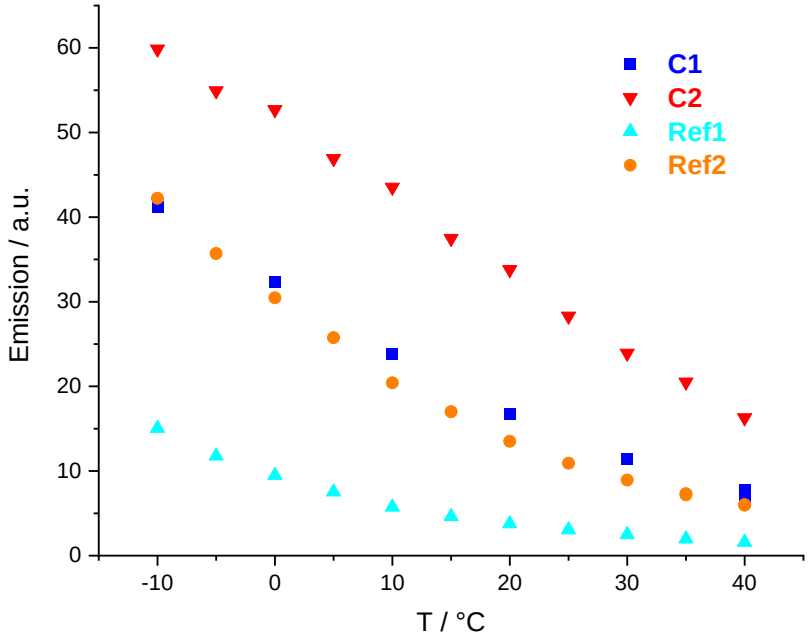

Figure S.I. 14. Temperature-dependence of the emission quantum yield of complexes **C1**, **C2**, **Ref1** and **Ref2** in inert-gas purged acetonitrile.

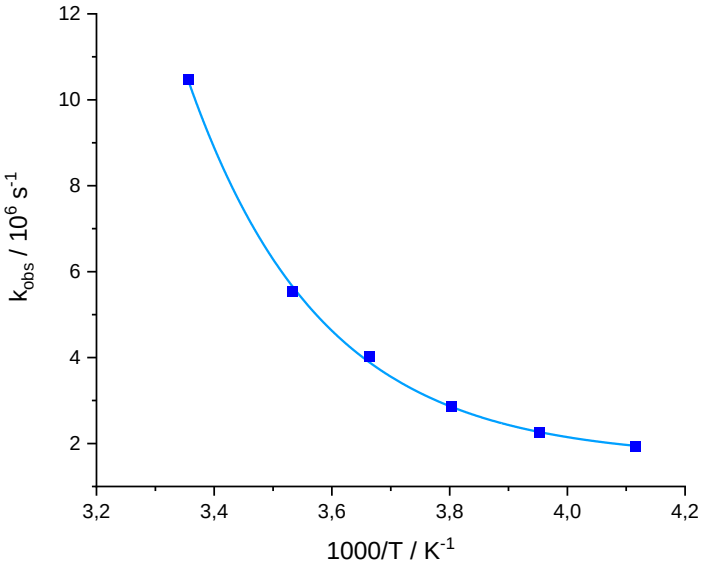

Figure S.I. 15. Plot of k_{obs} (1/τ) *vs.* 1000/T for **C1**. Curve fit according to Equation 2 of the manuscript.

S.I.-4 Electrochemistry

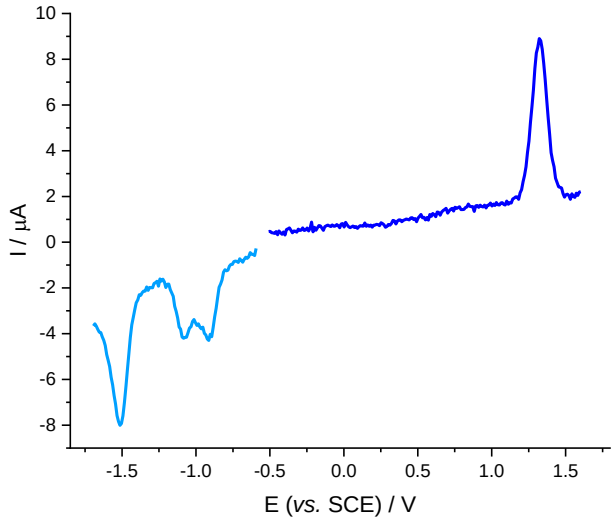

Figure S.I. 16. Square wave voltammogram of complex **C1** (0.25 mM) in dry acetonitrile under inert gas atmosphere, with 0.1 M $TBAPF_6$.

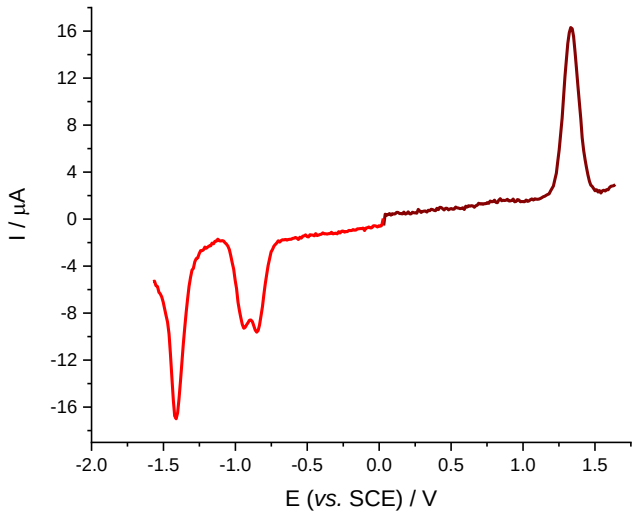

Figure S.I. 17. Square wave voltammogram of complex **C2** (0.5 mM) in dry acetonitrile under inert gas atmosphere, with 0.1 M $TBAPF_6$.

S.I.-5 Computational details

The calculations were made with Gaussian16 rev.B.01[4], using the PBE0 hybrid functional[5] with LanL2DZ[6-9] as basis set. The optimizations were conducted without symmetry constraints, followed by frequency calculations to confirm that energy minima had been reached in all cases. The energy, oscillator strength, and related MO contributions for the 100 lowest singlet–singlet and 10 lowest singlet–triplet excitations were obtained from the TD-DFT/singlets and the TD-DFT/triplets output files, respectively, for the S_0-optimized geometry. GaussView6, GaussSum3.3[10] and Chemissian4.53[11] were used for data analysis, visualization and surface plots. All calculations were conducted for acetonitrile solvated complexes using a conductor like polarized continuum (CPCM) solvation model.[12]

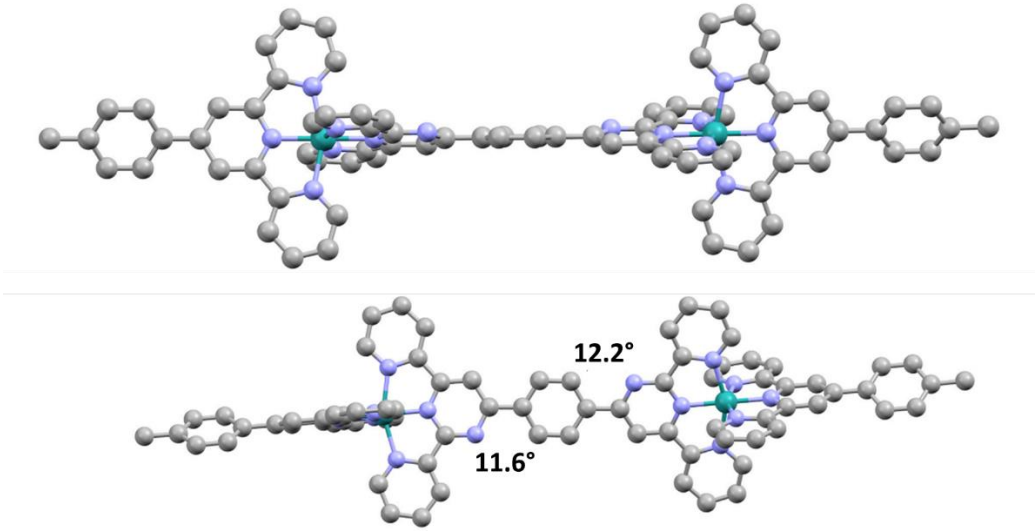

Figure S.I. 18. Optimized geometry of **C1** with 11.6° and 12.2° torsion angles of the phenyl bridge.

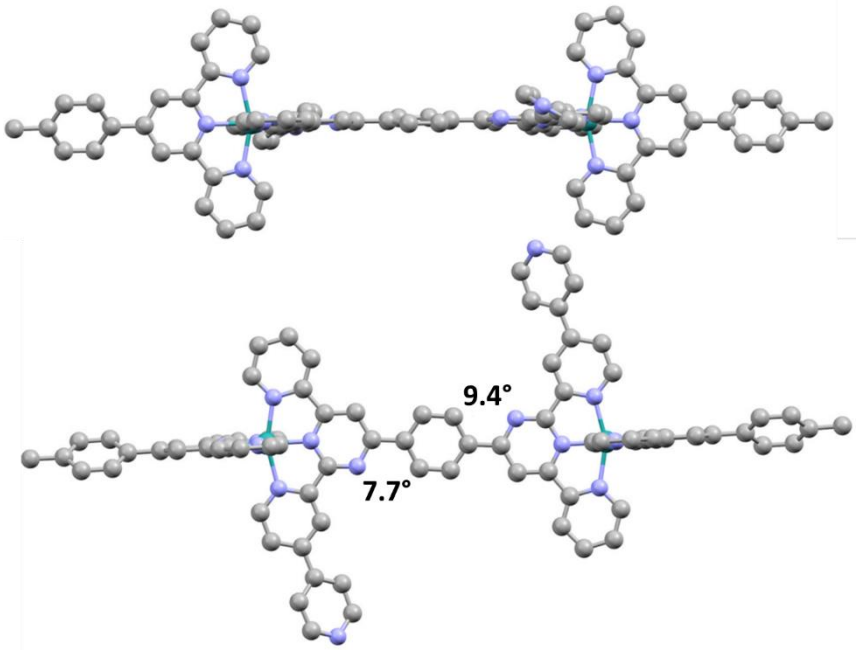

Figure S.I. 19. Optimized geometry of **C2** with 7.7° and 9.4° torsion angles of the phenyl bridge.

Table S.I. 1. Contributions to MOs for complexes **C1** and **C2**.

	C1			**C2**		
HOMO	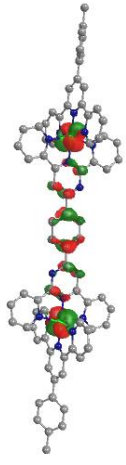	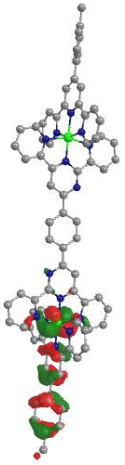	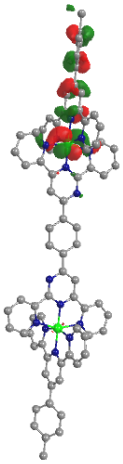	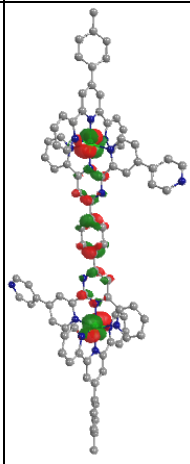	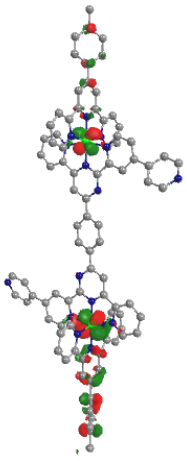	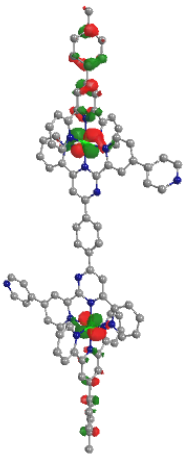
	-6.61 eV Ru: 61 % Tolyltpy: 8 % **L1**: 31 %	-6.63 eV Ru: 56 % Tolyltpy: 36 % **L1**: 8 %	-6.63 eV Ru: 56 % Tolyltpy: 36 % **L1**: 8 %	-6.64 eV Ru: 60 % Tolyltpy: 9 % **L2**: 31 %	-6.65 eV Ru: 55 % Tolyltpy: 37 % **L2**: 8 %	-6.65 eV Ru: 55 % Tolyltpy: 37 % **L2**: 8 %
LUMO	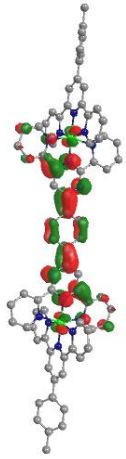		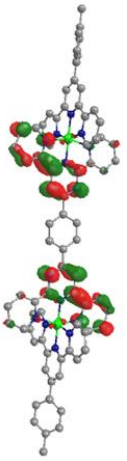	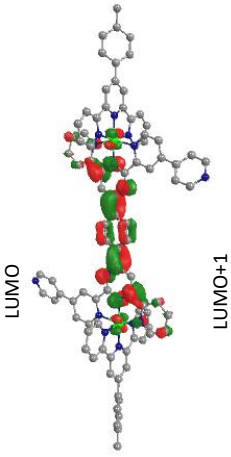	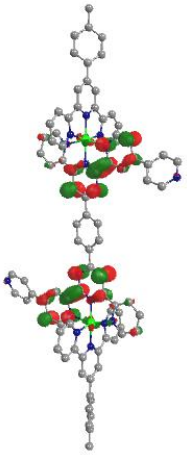	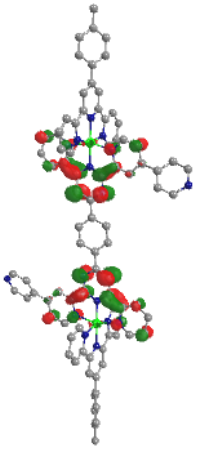
	-3.42 eV Ru: 9 % Tolyltpy: 1 % **L1**: 90 %		-3.04 eV Ru: 2 % Tolyltpy: 2 % **L1**: 96 %	-3.44 eV Ru: 9 % Tolyltpy: 1 % **L2**: 90 %	-3.09 eV Ru: 2 % Tolyltpy: 2 % **L2**: 96 %	-3.08 eV Ru: 2 % Tolyltpy: 2 % **L2**: 96 %

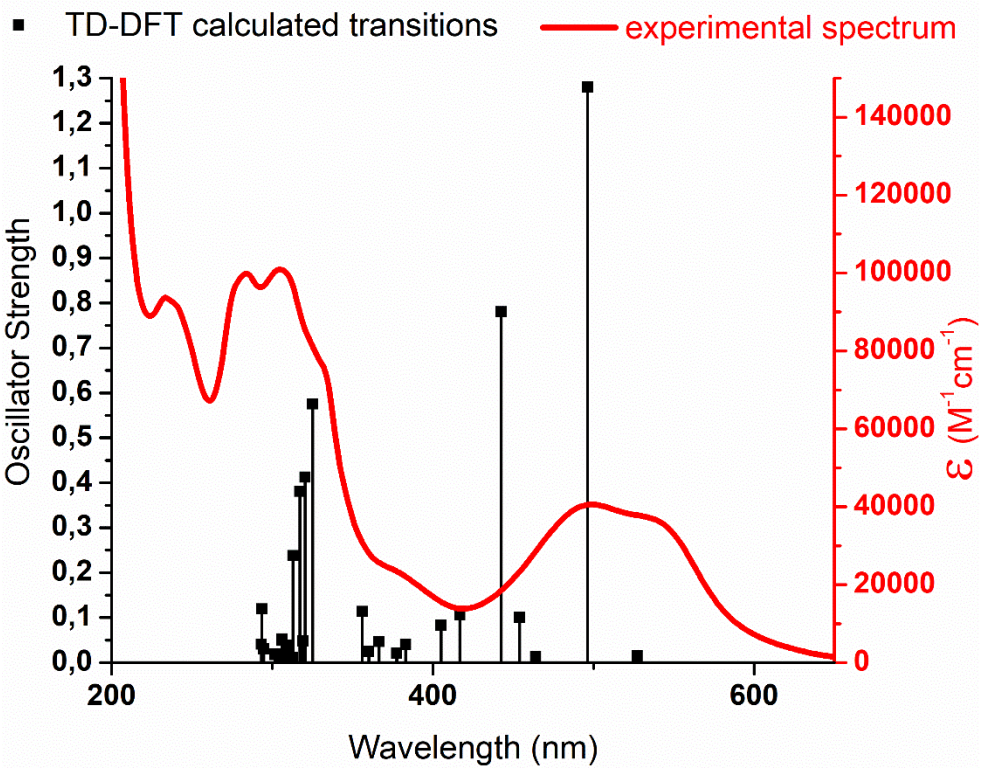

Figure S.I. 20. Comparison of the experimental absorption spectra with the predicted transitions (oscillator strength > 0.05) for complex **C1** in acetonitrile.

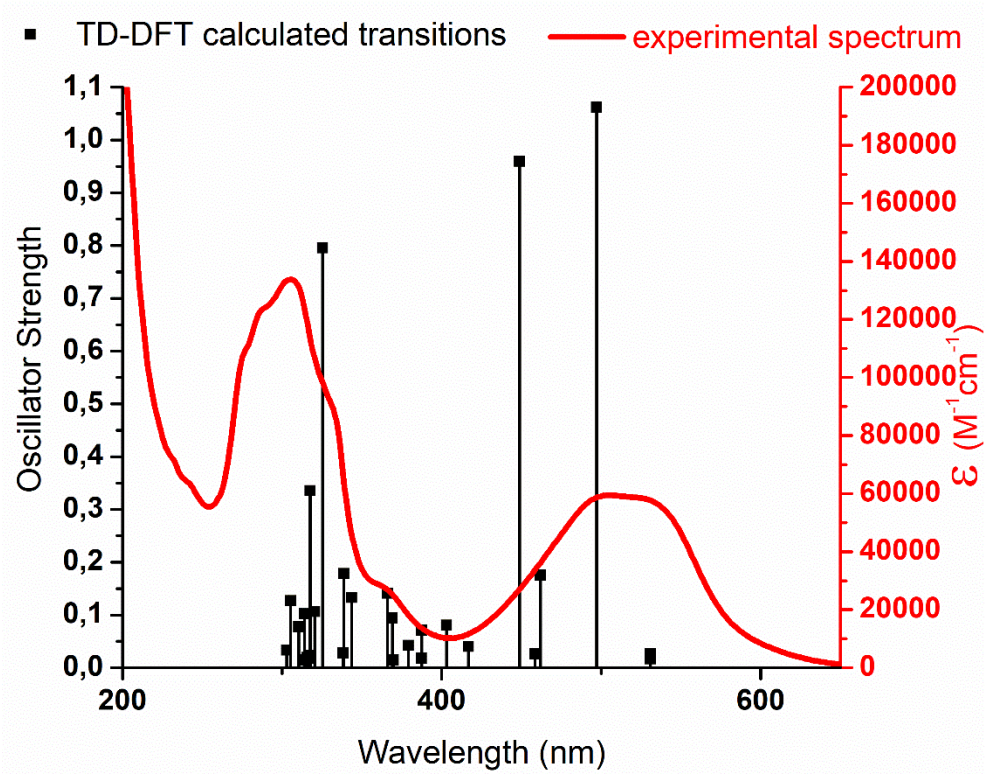

Figure S.I. 21. Comparison of the experimental absorption spectra with the predicted transitions (oscillator strength > 0.05) for complex **C2** in acetonitrile.

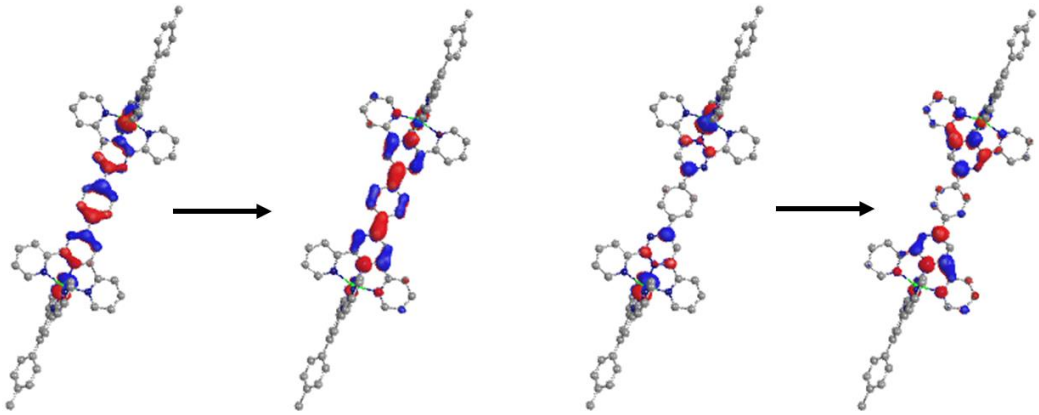

Figure S.I. 22. Natural transition analysis of the lowest singlet-triplet transition (= emissive state) of complex **C1**; (76/20, left/right).

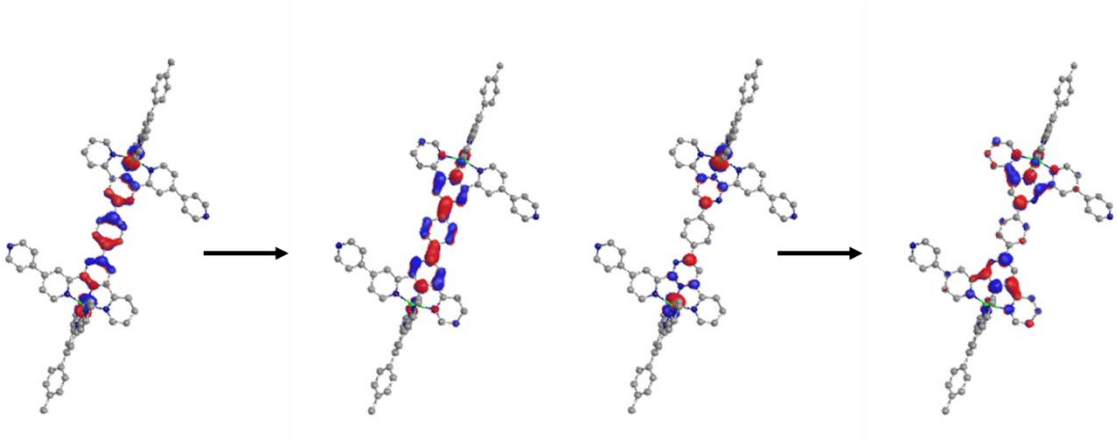

Figure S.I. 23. Natural transition analysis of the lowest singlet-triplet transition (= emissive state) of complex **C2**; (77/20, left/right).

Table S.I. 2. Atomic coordinates of the optimized geometry of **C1**.

Center	Atomic number	Coordinates (Angstroms)			Center	Atomic number	Coordinates (Angstroms)		
		X	Y	Z			X	Y	Z
1	7	9,580	0,002	-0,019	76	1	18,600	0,1703	-0,752
2	6	12,358	-0,113	0,037	77	1	18,559	-1,3714	0,109
3	6	10,237	-0,589	-1,053	78	1	18,605	0,1557	1,014
4	6	10,242	0,537	1,042	79	6	-2,890	-0,0944	0,149
5	6	11,636	0,488	1,091	80	7	-5,616	-0,1102	0,138
6	6	11,632	-0,655	-1,047	81	7	-3,566	0,6206	-0,799
7	1	12,164	0,890	1,948	82	6	-3,588	-0,8372	1,132
8	1	12,159	-1,100	-1,881	83	6	-4,983	-0,8340	1,103
9	6	9,327	-1,096	-2,095	84	6	-4,900	0,5945	-0,776
10	6	7,449	-1,972	-3,936	85	1	-3,056	-1,3841	1,897
11	7	7,985	-0,893	-1,852	86	6	-5,925	-1,5217	1,998
12	6	9,755	-1,740	-3,260	87	6	-7,867	-2,7300	3,554
13	6	8,810	-2,184	-4,192	88	7	-7,260	-1,3129	1,705
14	6	7,076	-1,323	-2,756	89	6	-5,537	-2,3339	3,067
15	1	10,811	-1,896	-3,442	90	6	-6,516	-2,9465	3,857
16	1	9,131	-2,685	-5,099	91	6	-8,200	-1,9094	2,472
17	1	6,034	-1,142	-2,525	92	1	-4,486	-2,4887	3,281
18	1	6,685	-2,299	-4,631	93	1	-9,233	-1,7219	2,209
19	6	9,337	1,116	2,049	94	1	-8,656	-3,1856	4,140
20	6	7,465	2,145	3,817	95	6	-5,750	1,3195	-1,732
21	6	9,769	1,720	3,234	96	6	-7,503	2,6082	-3,426
22	7	7,993	1,025	1,752	97	6	-5,236	2,1103	-2,760
23	6	7,087	1,531	2,621	98	7	-7,106	1,1657	-1,540
24	6	8,828	2,241	4,129	99	6	-7,957	1,8021	-2,377
25	1	10,827	1,785	3,459	100	6	-6,124	2,7664	-3,623
26	1	6,044	1,438	2,347	101	1	-4,162	2,1984	-2,868
27	1	9,153	2,712	5,050	102	1	-9,016	1,6596	-2,197
28	1	6,704	2,536	4,482	103	1	-8,223	3,0982	-4,070
29	44	7,591	0,083	-0,058	104	44	-7,591	-0,0678	0,071
30	7	5,616	0,163	-0,091	105	7	-9,580	-0,0222	0,004
31	6	2,891	0,175	-0,080	106	6	-12,358	0,0444	-0,094
32	6	4,987	1,230	-0,657	107	6	-10,242	0,9422	0,698
33	6	4,897	-0,850	0,460	108	6	-10,237	-0,9551	-0,736
34	7	3,564	-0,873	0,481	109	6	-11,631	-0,9388	-0,801
35	6	3,592	1,258	-0,662	110	6	-11,636	0,9928	0,664
36	1	3,061	2,097	-1,090	111	1	-12,155	-1,6638	-1,411
37	7	7,101	-1,705	0,898	112	1	-12,166	1,7436	1,237
38	6	6,109	-4,017	2,139	113	7	-7,993	1,5636	1,297
39	6	5,743	-1,913	1,022	114	6	-8,831	3,7041	2,892
40	6	7,948	-2,639	1,387	115	6	-7,089	2,3370	1,941
41	6	7,489	-3,804	2,011	116	6	-9,337	1,8406	1,435
42	6	5,225	-3,054	1,635	117	6	-9,772	2,9069	2,229
43	1	9,007	-2,445	1,272	118	6	-7,469	3,4140	2,745
44	1	8,206	-4,523	2,387	119	1	-6,045	2,0825	1,805
45	1	4,150	-3,169	1,706	120	1	-10,830	3,1157	2,332
46	7	7,266	1,897	-1,024	121	1	-6,708	4,0052	3,241
47	6	6,531	4,288	-2,288	122	1	-9,157	4,5331	3,509
48	6	8,209	2,750	-1,484	123	7	-7,984	-1,6804	-1,183
49	6	5,932	2,222	-1,187	124	6	-8,810	-3,7823	-2,834
50	6	5,549	3,411	-1,815	125	6	-9,327	-1,8956	-1,412
51	6	7,881	3,951	-2,119	126	6	-7,074	-2,4955	-1,765
52	1	9,241	2,459	-1,336	127	6	-7,448	-3,5548	-2,595
53	1	4,499	3,651	-1,933	128	6	-9,755	-2,9422	-2,235
54	1	8,673	4,602	-2,471	129	1	-6,032	-2,2895	-1,558
55	6	13,836	-0,174	0,066	130	1	-6,684	-4,1811	-3,040
56	6	16,685	-0,292	0,124	131	1	-10,813	-3,1024	-2,408
57	6	14,530	-1,242	-0,539	132	1	-9,131	-4,5963	-3,474
58	6	14,591	0,833	0,702	133	6	-13,836	0,0802	-0,147
59	6	15,988	0,773	0,728	134	6	-16,685	0,1486	-0,249
60	6	15,927	-1,300	-0,506	135	6	-14,537	1,2995	-0,039
61	1	13,982	-2,053	-1,010	136	6	-14,585	-1,1046	-0,304
62	1	14,094	1,685	1,159	137	6	-15,983	-1,0685	-0,350
63	1	16,547	1,566	1,219	138	6	-15,934	1,3302	-0,090
64	1	16,436	-2,142	-0,967	139	1	-13,994	2,2355	0,059
65	6	1,416	0,117	-0,036	140	1	-14,083	-2,0663	-0,358
66	6	-1,415	-0,040	0,097	141	1	-16,536	-1,9977	-0,458
67	6	0,782	-0,849	0,774	142	1	-16,449	2,2841	-0,011
68	6	0,609	0,997	-0,787	143	6	-18,190	0,1879	-0,330
69	6	-0,782	0,916	-0,724	144	1	-18,636	-0,7374	0,049
70	6	-0,608	-0,925	0,843	145	1	-18,520	0,3070	-1,371
71	1	1,395	-1,537	1,345	146	1	-18,601	1,0278	0,240
72	1	1,051	1,744	-1,439	147	1	6,248	5,2136	-2,776
73	1	-1,395	1,592	-1,309	148	1	-6,230	-3,5785	4,690
74	1	-1,050	-1,690	1,472	149	1	5,730	-4,9113	2,620
75	6	18,192	-0,340	0,130	150	1	-5,748	3,3862	-4,429

Table S.I. 3. Atomic coordinates of the optimized geometry of **C2**.

Center	Atomic number	Coordinates (Angstroms)			Center	Atomic number	Coordinates (Angstroms)		
		X	Y	Z			X	Y	Z
1	7	9.568	0.529	-0.033	85	1	4.057	-5.278	1.261
2	6	12.348	0.545	-0.058	86	1	7.581	-6.452	-0.975
3	6	10.217	0.508	-1.228	87	1	6.768	-8.789	-0.847
4	6	10.238	0.558	1.149	88	1	3.382	-7.662	1.267
5	6	11.634	0.562	1.161	89	6	-2.876	-0.336	0.043
6	6	11.612	0.520	-1.263	90	7	-5.599	-0.485	0.020
7	1	12.169	0.554	2.102	91	7	-3.617	0.812	0.061
8	1	12.131	0.533	-2.214	92	6	-3.507	-1.603	0.010
9	6	9.299	0.482	-2.379	93	6	-4.901	-1.654	-0.001
10	6	7.407	0.431	-4.404	94	6	-4.946	0.706	0.049
11	7	7.957	0.477	-2.061	95	1	-2.925	-2.513	-0.020
12	6	9.720	0.462	-3.712	96	6	-5.780	-2.831	-0.039
13	6	8.768	0.437	-4.738	97	6	-7.612	-4.903	-0.113
14	6	7.041	0.451	-3.056	98	7	-7.133	-2.545	-0.048
15	1	10.776	0.466	-3.951	99	6	-5.320	-4.150	-0.067
16	1	9.083	0.421	-5.775	100	6	-6.243	-5.202	-0.104
17	1	6.000	0.447	-2.760	101	6	-8.018	-3.566	-0.084
18	1	6.638	0.411	-5.166	102	1	-4.256	-4.357	-0.059
19	6	9.341	0.573	2.317	103	1	-9.068	-3.300	-0.090
20	6	7.485	0.608	4.376	104	1	-8.359	-5.687	-0.141
21	6	9.785	0.605	3.642	105	6	-5.860	1.857	0.069
22	7	7.993	0.558	2.023	106	6	-7.709	3.889	0.093
23	6	7.095	0.576	3.035	107	6	-5.414	3.175	0.106
24	6	8.852	0.622	4.685	108	7	-7.200	1.537	0.046
25	1	10.846	0.618	3.862	109	6	-8.097	2.550	0.058
26	1	6.049	0.566	2.758	110	6	-6.342	4.232	0.120
27	1	9.185	0.647	5.716	111	1	-4.344	3.350	0.104
28	1	6.730	0.621	5.151	112	1	-9.144	2.275	0.044
29	44	7.576	0.510	-0.015	113	1	-8.480	4.650	0.123
30	7	5.600	0.487	0.001	114	6	-5.899	5.644	0.162
31	6	2.877	0.343	0.023	115	7	-5.053	8.348	0.246
32	6	4.904	1.659	-0.014	116	6	-4.696	6.014	0.794
33	6	4.945	-0.702	0.032	117	6	-6.666	6.669	-0.425
34	7	3.616	-0.806	0.041	118	6	-6.209	7.990	-0.361
35	6	3.511	1.609	0.001	119	6	-4.317	7.361	0.813
36	1	2.931	2.521	0.005	120	1	-4.067	5.281	1.288
37	7	7.198	-1.537	0.029	121	1	-7.592	6.454	-0.948
38	6	6.335	-4.230	0.097	122	1	-6.784	8.792	-0.813
39	6	5.857	-1.855	0.051	123	1	-3.397	7.666	1.300
40	6	8.093	-2.551	0.040	124	44	-7.575	-0.511	-0.005
41	6	7.702	-3.890	0.072	125	7	-9.566	-0.532	-0.034
42	6	5.408	-3.172	0.085	126	6	-12.347	-0.552	-0.074
43	1	9.140	-2.279	0.028	127	6	-10.243	-0.566	1.145
44	1	8.471	-4.653	0.101	128	6	-10.209	-0.509	-1.232
45	1	4.338	-3.345	0.081	129	6	-11.604	-0.522	-1.275
46	7	7.138	2.545	-0.052	130	6	-11.639	-0.572	1.148
47	6	6.253	5.204	-0.098	131	1	-12.117	-0.533	-2.229
48	6	8.025	3.565	-0.081	132	1	-12.179	-0.568	2.087
49	6	5.786	2.834	-0.044	133	7	-8.003	-0.566	2.030
50	6	5.327	4.154	-0.067	134	6	-8.875	-0.642	4.688
51	6	7.621	4.903	-0.105	135	6	-7.110	-0.587	3.047
52	1	9.074	3.297	-0.086	136	6	-9.352	-0.585	2.317
53	1	4.264	4.362	-0.063	137	6	-9.803	-0.623	3.640
54	1	8.370	5.685	-0.128	138	6	-7.507	-0.624	4.385
55	6	13.828	0.554	-0.072	139	1	-6.062	-0.573	2.776
56	6	16.680	0.568	-0.097	140	1	-10.865	-0.639	3.853
57	6	14.547	-0.083	-1.104	141	1	-6.756	-0.639	5.165
58	6	14.559	1.196	0.950	142	1	-9.214	-0.672	5.717
59	6	15.958	1.202	0.934	143	7	-7.945	-0.471	-2.053
60	6	15.946	-0.077	-1.112	144	6	-8.741	-0.423	-4.734
61	1	14.020	-0.616	-1.891	145	6	-9.285	-0.478	-2.378
62	1	14.041	1.718	1.749	146	6	-7.024	-0.441	-3.043
63	1	16.497	1.710	1.729	147	6	-7.382	-0.416	-4.393
64	1	16.476	-0.588	-1.912	148	6	-9.699	-0.454	-3.714
65	6	1.408	0.188	0.031	149	1	-5.984	-0.436	-2.742
66	6	-1.408	-0.178	0.047	150	1	-6.609	-0.393	-5.151
67	6	0.846	-1.092	0.220	151	1	-10.754	-0.459	-3.958
68	6	0.537	1.283	-0.148	152	1	-9.051	-0.405	-5.773
69	6	-0.845	1.102	-0.138	153	6	-13.826	-0.561	-0.095
70	6	-0.537	-1.274	0.229	154	6	-16.678	-0.581	-0.136
71	1	1.507	-1.938	0.363	155	6	-14.562	-1.210	0.919
72	1	0.921	2.284	-0.312	156	6	-14.541	0.075	-1.131
73	1	-1.507	1.948	-0.280	157	6	-15.940	0.064	-1.148
74	1	-0.921	-2.274	0.392	158	6	-15.960	-1.221	0.895
75	6	18.187	0.600	-0.126	159	1	-14.047	-1.739	1.716
76	1	18.546	1.477	-0.680	160	1	-14.011	0.606	-1.916
77	1	18.596	-0.288	-0.619	161	1	-16.467	0.568	-1.954
78	1	18.606	0.658	0.884	162	1	-16.502	-1.741	1.680
79	6	5.890	-5.642	0.136	163	6	-18.185	-0.569	-0.142
80	7	5.037	-8.344	0.213	164	1	-18.581	-0.511	-1.161
81	6	4.685	-6.011	0.766	165	1	-18.569	0.301	0.407
82	6	6.655	-6.667	-0.453	166	1	-18.595	-1.463	0.338
83	6	6.195	-7.987	-0.393	167	1	5.912	6.233	-0.116
84	6	4.304	-7.358	0.781	168	1	-5.900	-6.230	-0.126

S.I.-6 Hydrogen production experiments

Hydrogen evolution was monitored using a Perkin Elmer Clarus-480 gas chromatograph (GC) with a thermal conductivity detector, argon as carrier and eluent gas, a 7 ft. HayeSep N 60/80 pre-column, a 9 ft. molecular sieve 13 x 45/60 column and a 2 mL injection loop. Three distinct solutions for the sacrificial electron donor and proton source, the photosensitizer and the catalyst were prepared and mixed together to obtain 5 mL of solutions in standard 20 mL headspace vials. Using DMF as a solvent, the resulting molar concentration of photocatalytic medium are: 1 M for triethanolamine (TEOA), 0.1 M for HBF_4, 0.56 M for water ($pH_{apparent}$= 8.9). The concentration of active species were: 0.1 mM for the photosensitizer, 1 mM of cobalt pre-catalyst ($[Co(H_2O)_6](BF_4)_2$) or cobalt catalyst $[Co(dmgH)_2(py)Cl]$ and 6 mM of dimethylglyoxime.

The vials were placed on top of a 450 nm (blue-light irradiation) or a 630 nm (red-light irradiation) centered LED set to an approximate 62 mW (blue light) or 45 mW (red light) output, in an aluminum cast connected to a thermostatic bath set at 20 °C. They were sealed with a rubber septum pierced with two stainless steel tubes. The first tube carried an argon flow pre-bubbled in DMF. The flow was set between 5 mL/min and 10 mL/min (adjusted with calibrated mass flow MCseries from Alicat) and referenced with a digital flowmeter (Perkin Elmer FlowMark) depending on the sample. The second tube led the flow to the GC sample loop through a 2 mL overflow protection vial, then through an 8-port stream select valve (VICCI) and finally to GC sample loop. A microprocessor (Arduino Uno) coupled with a custom PC interface allowed for timed injections. For calibration of the H_2 production rate at a specific argon flow, a syringe pump (New Era Pump) equipped with a gas-tight syringe (SGE) and a 26s gauge needle (Hamilton) was used to bubble different rates of pure hydrogen gas into the sample, to a minimum of 0.5 µL/minute. This gave a linear fit for the peak area of H_2 *vs.* the flow rates of H_2. For calibration testing, stock cylinders of known concentration of H_2 in argon replaced the argon flow (inserted at the pre-bubbler, to keep the same vapor matrix). The measured results, independent of flow rate (under same pressure) can be easily converted into a rate of hydrogen production following Equation S.I. 5. The errors associated to the *TON* (turn-over number) and *TOF* (turn-over frequency) were estimated to be within 10 %.[13]

H_2 rate (µL/min) = [H_2 standard] (ppm) × Ar flow rate (mL/min) Equation S.I. 2

H_2 rate (nmol/min) = H_2 rate (µL/min) / 24.45 × 1000 Equation S.I. 3

TOF ($mmol_{H2}.mol_{PS}^{-1}.min^{-1}$) = H_2 rate (nmol/min) / n_{PS} (mol) / 10^6 Equation S.I. 4

The amount of hydrogen produced between two injections is calculated using the average rate over that period of time [t_i ; t_j], multiplied by the time between two injections (tj-ti).

$n_{H2\ total}$ (nmol) = $\sum_{t0}^{tf} n_{H2}[ti\ ;\ tj]$ = $\sum_{t0}^{tf}$((H_2 rate (ti) + H_2 rate (tj)) /2) × (tj-ti)) Equation S.I. 5

For a chosen length of experiment (t_f) TON(t_f) = $n_{H2(tf)}$ / n_{PS} Equation S.I. 6

A Savitzky-Golay smoothing with software Origin was applied for the data of TOFs.

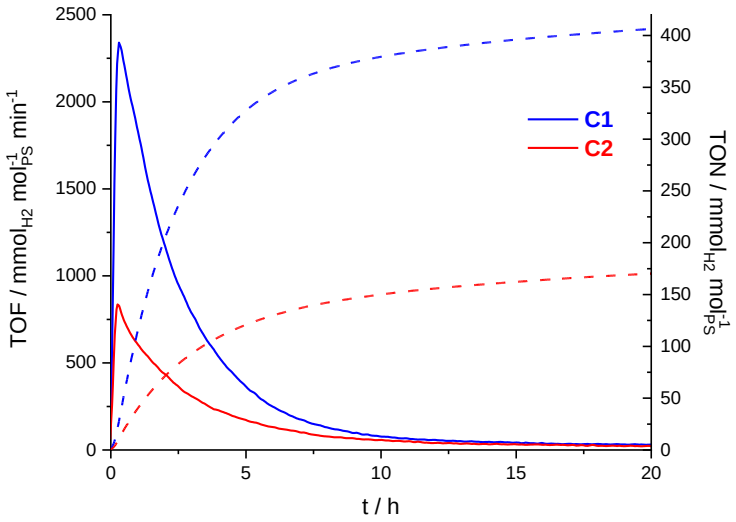

Figure S.I. 24. Hydrogen production of dinuclear complexes **C1** and **C2** as PS (0.1 mM) under blue-light irradiation (LED centered at 445 nm); using $[Co(dmgH)_2(py)Cl]$ as catalyst (1 mM), $dmgH_2$ (6 mM), TEOA as sacrificial electron donor (1 M) and HBF_4 as proton source (0.1 M) in DMF; TOF: solid lines; TON: dashed lines.

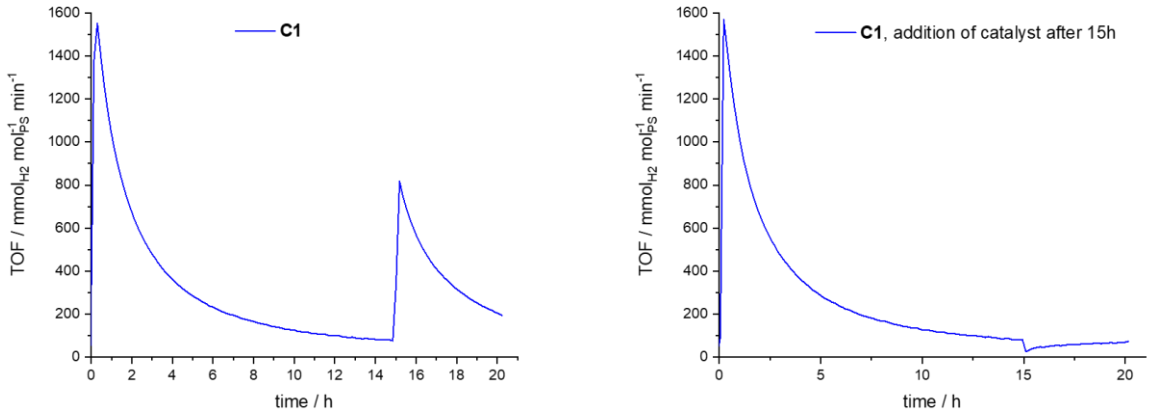

Figure S.I. 25. Hydrogen production of dinuclear complex **C1** as PS (0.1 mM) under blue-light irradiation (LED centered at 445 nm); using $[Co(H_2O)_6](BF_4)_2$ as pre-catalyst (1 mM), $dmgH_2$ (6 mM), TEOA as sacrificial electron donor (1 M) and HBF_4 as proton source (0.1 M) in DMF; left: addition of same amount of **C1** in 0.25 ml DMF after 15 h; right: addition of same amount of $[Co(H_2O)_6](BF_4)_2$ and $dmgH_2$ in 0.25 mL DMF after 15 h.

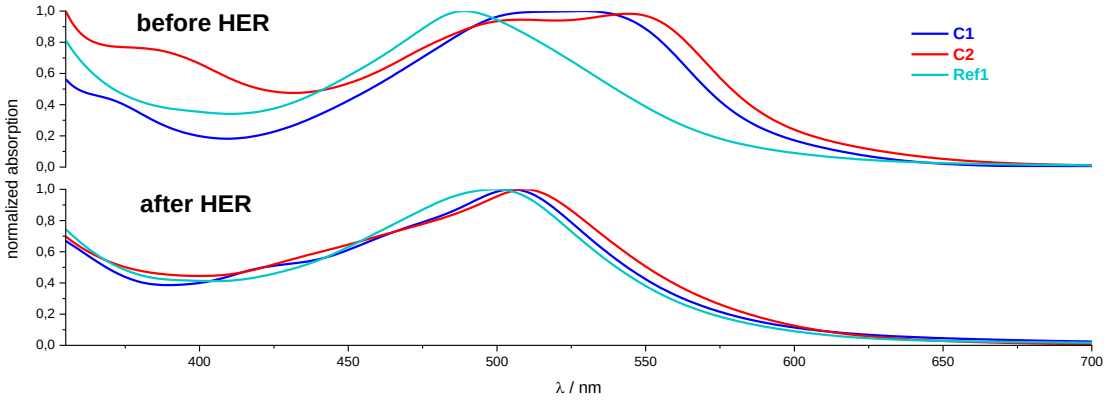

Figure S.I. 26. UV-is absorption spectra of DMF solutions containing **C1, C2** or **Ref1** (0.1 mM); $[Co(H_2O)_6](BF_4)_2$ (1 mM), $dmgH_2$ (6 mM), TEOA (1 M) and HBF_4 (0.1 M) before (upper graph) and after (lower graph) 23 h under blue-light irradiation (LED centered at 445 nm).

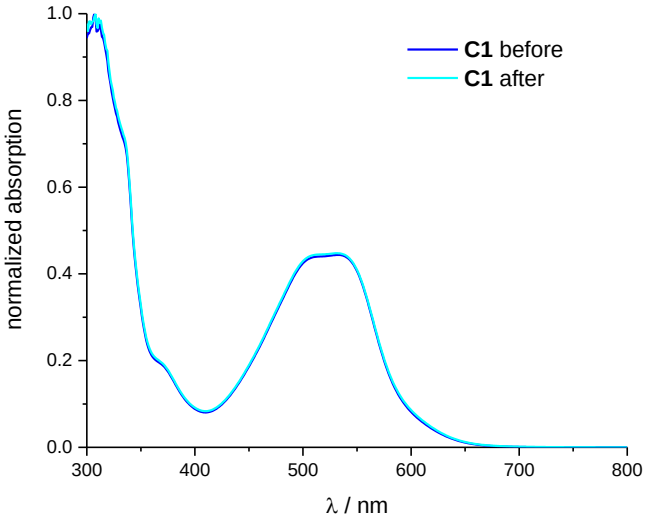

Figure S.I. 27. UV-is absorption spectra of **C1** in DMF (0.1 mM) before and after 18 h under blue-light irradiation (LED centered at 445 nm).

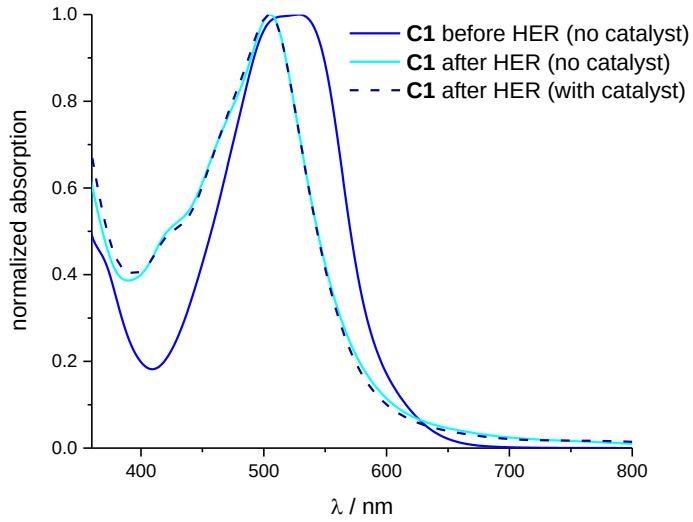

Figure S.I. 28. UV-is absorption spectra of DMF solutions containing **C1** (0.1 mM), TEOA (1 M) and HBF_4 (0.1 M) before and after 18 h under blue-light irradiation (LED centered at 445 nm) (solid lines), and of a DMF solution containing **C1** (0.1 mM), $[Co(H_2O)_6](BF_4)_2$ (1 mM), $dmgH_2$ (6 mM), TEOA (1 M) and HBF_4 (0.1 M) after 18 h under blue light irradiation (dashed line).

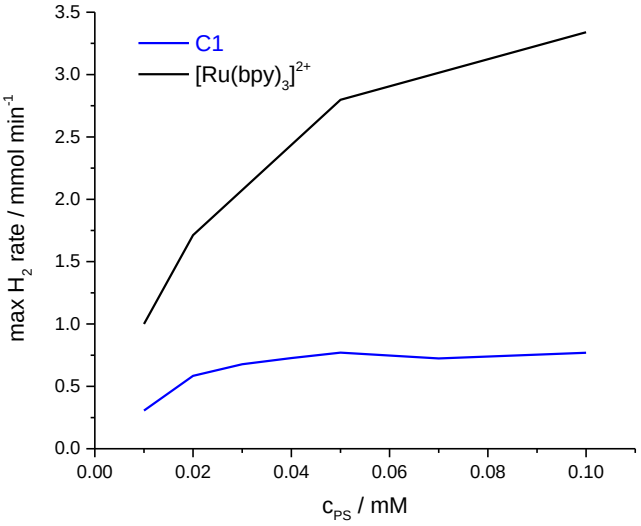

Figure S.I. 29. Maximum hydrogen production rate of dinuclear complex **C1** in comparison with $[Ru(bpy)_3]^{2+}$ for different concentrations of PS in a DMF solution with $[Co(H_2O)_6](BF_4)_2$ as pre-catalyst (1 mM), $dmgH_2$ (6 mM), TEOA as sacrificial electron donor (1 M) and HBF_4 as proton source (0.1 M) under blue-light irradiation (LED centered at 445 nm).

S.I.-7 References

1. J. N. Demas and G. A. Crosby, *J. Phys. Chem.*, 1971, **75**, 991-1024.
2. K. E. Spettel and N. H. Damrauer, *J. Phys. Chem. A*, 2014, **118**, 10649-10662.
3. N. G. Connelly and W. E. Geiger, *Chem. Rev.*, 1996, **96**, 877-910.
4. M. J. Frisch, G. W. Trucks, H. B. Schlegel, G. E. Scuseria, M. A. Robb, J. R. Cheeseman, G. Scalmani, V. Barone, G. A. Petersson, H. Nakatsuji, X. Li, M. Caricato, A. V. Marenich, J. Bloino, B. G. Janesko, R. Gomperts, B. Mennucci, H. P. Hratchian, J. V. Ortiz, A. F. Izmaylov, J. L. Sonnenberg, Williams, F. Ding, F. Lipparini, F. Egidi, J. Goings, B. Peng, A. Petrone, T. Henderson, D. Ranasinghe, V. G. Zakrzewski, J. Gao, N. Rega, G. Zheng, W. Liang, M. Hada, M. Ehara, K. Toyota, R. Fukuda, J. Hasegawa, M. Ishida, T. Nakajima, Y. Honda, O. Kitao, H. Nakai, T. Vreven, K. Throssell, J. A. Montgomery Jr., J. E. Peralta, F. Ogliaro, M. J. Bearpark, J. J. Heyd, E. N. Brothers, K. N. Kudin, V. N. Staroverov, T. A. Keith, R. Kobayashi, J. Normand, K. Raghavachari, A. P. Rendell, J. C. Burant, S. S. Iyengar, J. Tomasi, M. Cossi, J. M. Millam, M. Klene, C. Adamo, R. Cammi, J. W. Ochterski, R. L. Martin, K. Morokuma, O. Farkas, J. B. Foresman and D. J. Fox, *Journal*, 2016.
5. C. Adamo and V. Barone, *J. Chem. Phys.*, 1999, **110**, 6158-6170.
6. T. H. Dunning Jr and P. J. Hay, *Mordern Theoretical Chemistry III ed.*, Plenum, New york, 1977.
7. P. J. Hay and W. R. Wadt, *J. Chem. Phys.*, 1985, **82**, 270-283.
8. P. J. Hay and W. R. Wadt, *J. Chem. Phys.*, 1985, **82**, 299-310.
9. W. R. Wadt and P. J. Hay, *J. Chem. Phys.*, 1985, **82**, 284-298.
10. N. M. O'Boyle, A. L. Tenderholt and K. M. Kangner, *J. Comput. Chem.*, 2008, **29**, 839-845.
11. S. Leonid, *V 4.53*, 2005-2017, www.chemissian.com.
12. M. Cossi, N. Rega, G. Scalmani and V. Barone, *J. Comput. Chem.*, 2003, **24**, 669-681.
13. C. Lentz, O. Schott, T. Auvray, G. Hanan and B. Elias, *Inorg. Chem.*, 2017, **56**, 10875-10881.